2.2 X-RAY ABSORPTION SPECTROSCOPY OF EMBEDDED AND EXTRACTED NANO-OXIDES IN NANOSTRUCTURED FERRITIC ALLOY MA957—T. Stan, G.R. Odette (University of California Santa Barbara), D. Sprouster, A. Ofran, L. Ecker (Brookhaven National Laboratory)

OBJECTIVE

The objective of this work is to use x-ray absorption spectroscopy to characterize the Y-Ti-O nano-oxides in NFA MA957.

SUMMARY

The chemistries and structures of both embedded and extracted Y-Ti-O nanometer-scale oxides in nanostructured ferritic alloy (NFA) MA957 were characterized by x-ray absorption spectroscopy (XAS). $Y_2Ti_2O_7$ is the primary embedded phase, while the slightly larger extracted oxides are primarily Y_2TiO_5. Analysis of the embedded nano-oxides in MA957 is difficult partly due to the multiple Ti environments associated with different oxides and those still residing in matrix lattice sites. Thus, bulk extraction followed by selective filtration was used to isolate the larger Y_2TiO_5 oxides for XAS. The smaller $Y_2Ti_2O_7$ oxides passed through the filters but were the predominant embedded phase.

PROGRESS AND STATUS

Introduction

Nanostructured ferritic alloys (NFAs) are a developmental class of oxide dispersion strengthened steels (ODS) with potential applications in nuclear fission and fusion energy systems [1–4]. NFAs are thermally stable, have excellent high-temperature creep strength and are uniquely irradiation tolerant. NFAs are typically processed by ball-milling Fe–14Cr–W–Ti metallic powders with yttria (Y_2O_3) powders followed by hot consolidation leading to the precipitation of Y-Ti-O nano-oxides (NOs) that impede dislocation motion, enhance defect recombination and trap transmutation produced He in small high-pressure gas bubbles. The NO character (size, number density, composition, and structure) depends on the alloy composition and processing history. NOs have been studied using transmission electron microscopy (TEM) [5–11], atom probe tomography (APT) [12–16], as well as small angle neutron and x-ray scattering (SANS and SAXS) [8,17,18]. These studies have been interpreted to show NOs that range from solute enriched clusters with core-shell structures to various complex oxides, such as pyrochlore $Y_2Ti_2O_7$ and orthorhombic Y_2TiO_5.

A reference heat of INCO NFA MA957 with a nominal composition of 14.9Cr, 1.1Ti, 0.17Mo, 0.13Y, 0.88O, bal. Fe (at%), along with trace impurity elements such as Al, Mn, Si and C [19] was examined in this study. Previous TEM and SANS studies indicate NO averages for number densities of $N \sim 5 \times 10^{23}$ m^{-3}, average diameters $\langle d \rangle \sim 2.5$ nm, and volume fractions of $\langle f \rangle \sim 0.4\%$ [20]. The smallest ($d < 5$ nm) NOs were found to be primarily cubic pyrochlore $Y_2Ti_2O_7$, while larger ($d > 6$ nm) NOs were primarily orthorhombic Y_2TiO_5. Larger ($d > 50$ nm) Y_2O_3, TiO_x, Mo-rich, and C-rich precipitates were also observed. Given the low fraction and ultra-small NO size, a synchrotron light source is needed to obtain reliable x-ray measurements. As a complement to x-ray diffraction (XRD) and SAXS measurements, the National Synchrotron Light Source (NSLS) was used to carry out x-ray absorption spectroscopy (XAS) studies.

One challenge to XAS on MA957 is that it contains a large amount of Ti with ≈ 2/3 of the total left in solution and only 1/3 contained in the oxides [21]. A previous XAS study by Liu et al. indicated nearly equal amounts of $Y_2Ti_2O_7$, Y_2TiO_5, and Y_2O_3 [22]. However, the remaining dissolved Ti complicated the XAS analysis. Here, we build on this work using a bulk extraction method to remove the matrix and isolate one of the NOs of interest.

Experimental

The steps involved in the bulk extraction procedure used to isolate the NOs are outlined in Fig. 1. MA957 was placed in a platinum wire mesh (Figure 1a) and submerged into a 1 L solution composed of 100 mL acetyl acetone, 10 g of tetra methyl ammonium chloride, with a balance of methanol. A 20 V potential was used to dissolve the MA957 matrix. The non-acetic solution is dark red at the end of the 24 h process (Figure 1b). A 100 nm-pore filter was then used to remove larger particles (not shown in Figure 1). The remaining liquid was drained through a polysulfone 10 nm-pore filter for 50 h. Filtering was accelerated by connecting a fume-hood vacuum under the filtration capsule (Figure 1c). The filter containing NOs was used for XAS measurements (Figure 1d). This procedure yields a roughly uniform distribution of NOs on top of the filter, which is ideal for fluorescence-mode XAS analysis.

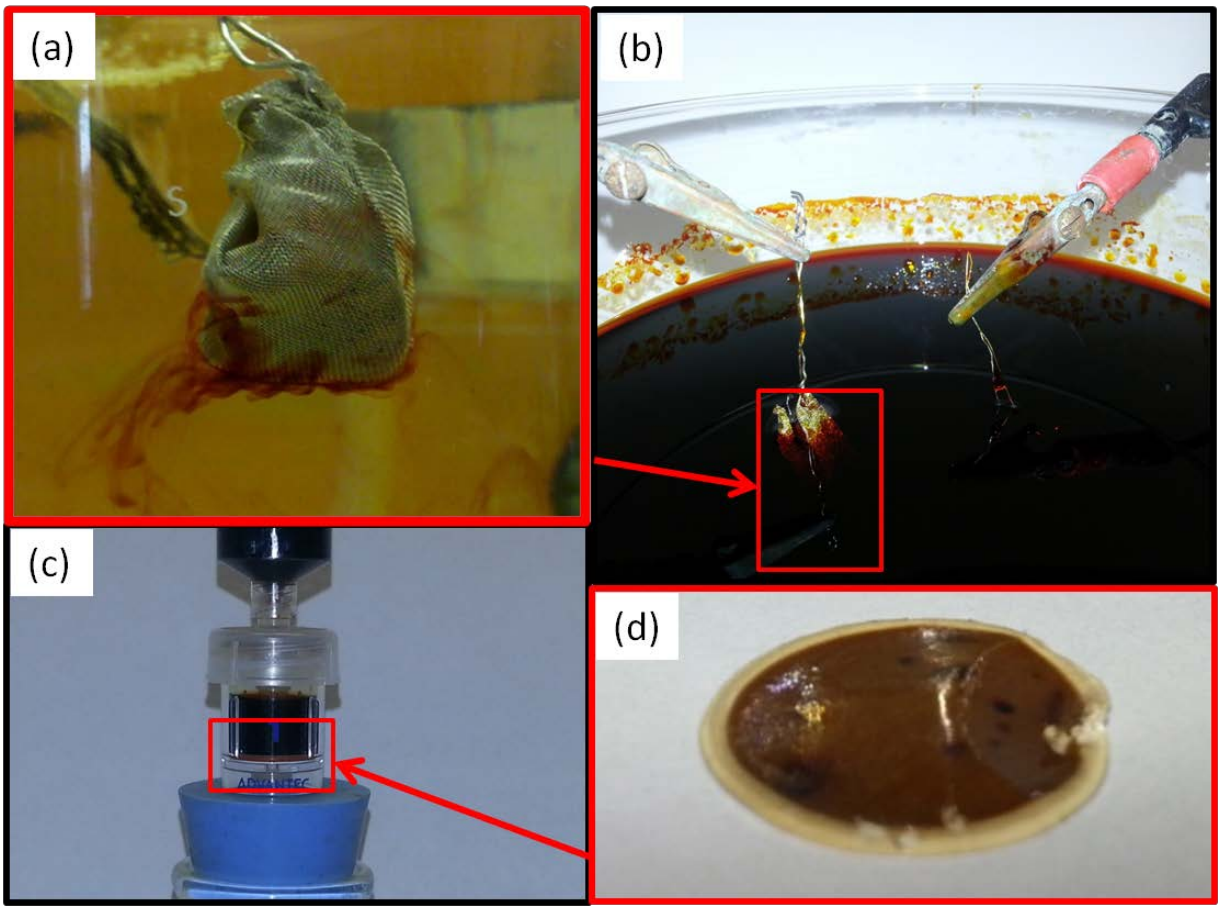

Figure 1. (a) MA957 in platinum wire mesh being dissolved; (b) The initially clear yellow liquid is dark red at the end of the process; the liquid is then pre-treated by 100 nm-pore filtration (not shown); (c) a vacuum under a 10 nm-pore filter is used to accelerate the process; and, (d) the filter containing NOs is removed and used for XAS measurements.

Both as-received MA957 alloy containing embedded NOs, and filters containing selectively extracted NOs, were studied using XAS fluorescence and transmission-mode measurements at beamline X23A2 of the NSLS at Brookhaven National Laboratory. Ambient temperature XAS spectra were measured at the Ti and Y *K*-edges (4.492 keV and 17.038 keV, respectively), at a photoelectron wavenumber (*k)* value of 13 $Å^{-1}$. Ti metal and Y_2O_3 powder were simultaneously measured in transmission mode for energy

calibration. Background subtraction, spectra alignment, and normalization of the extended x-ray absorption fine structure (EXAFS) data were carried out using the ATHENA code [23]. The positions of the Ti and Y edges were determined from the reference absorption spectra using known features. Isolated EXAFS spectra were then Fourier Transformed (FT) over a *k* range of 3.0 – 11 $Å^{-1}$ and back FT over a non-phase-corrected radial distance of 0.9 – 2.4 Å to isolate the first nearest neighbor (NN) atomic shell. Structural parameters were then determined using the model-independent, or log-ratio, method [24]. The model-dependent method (using a combination of Artemis, IFEFFIT and FEFF) was found to be difficult due to the disorder and weak signals present in the samples. The changes in the coordination number (N), bond length (ΔBL), Debye – Waller factor ($\Delta\sigma^2$) and asymmetry parameter (ΔC_3), relative to the bulk standards, were allowed to vary during the fitting. Fitting of the log-ratio of amplitude and phase-difference of the isolated first shell was performed over a *k* range of ~3 – 10 $Å^{-1}$ (depending on the edge) with multiple k-weights to reduce inter-parameter correlations.

Results

The XAS spectra are plotted as absorption versus x-ray energy, and consist of an x-ray absorption near edge structure (XANES) region with a broad edge and, in some cases, a pre-edge peak at lower energy, and an extended x-ray absorption fine structure (EXAFS) oscillating region at energies beyond the edge. The Ti and Y *K*-edge XANES spectra are shown in Figure 2 for the embedded and extracted oxides, along with those for bulk standards. In Figure 2 and Figure 3, some curves have been vertically offset for clarity. The pre-edge peaks and broad features observed in the XANES spectra result from multiple-scattering resonances, and can be used to identify the crystallographic phase, symmetry and oxidation state of the metal ions [25,26]. At the Ti edge in Figure 2a, the Ti atoms in the bulk (embedded) MA957 show a complex mixture of environments, similar to metallic Ti, $Y_2Ti_2O_7$ and TiO. Note the higher intensity in the 4.99 – 5.02 keV range and subtle shifts relative to the bulk standards. In contrast, the extracted NOs show a sharp pre-edge resonance that is more characteristic of the Y_2TiO_5 phase. Additionally, the general shape and the features in the near-edge peak (~4.98 – 5.0 keV) are also most similar to the Y_2TiO_5 phase. These broad features in the XANES spectra may suggest a degree of structural disorder in the extracted NOs due to their relatively small size and complex chemistry. This observation is consistent with other NO studies, where changes in the XANES regions from structural and chemical disorder are reported [27].

The XANES spectra at the Y edge (Figure 2b) show features for the embedded NOs that are almost identical to the $Y_2Ti_2O_7$ standard. A small Y_2O_3 component may also be present in the embedded NOs as indicated by a subtle increase in intensity between 17.05 – 17.07 keV and 17.10 – 17.12 keV, where Y_2O_3 has similar XANES features. The spectra for the extracted NO again show very broad features that are more consistent with the Y_2TiO_5 phase. Further, the features observed in the XANES Y edge for the extracted NOs are consistent with the Ti edge data and a disordered atomic environment.

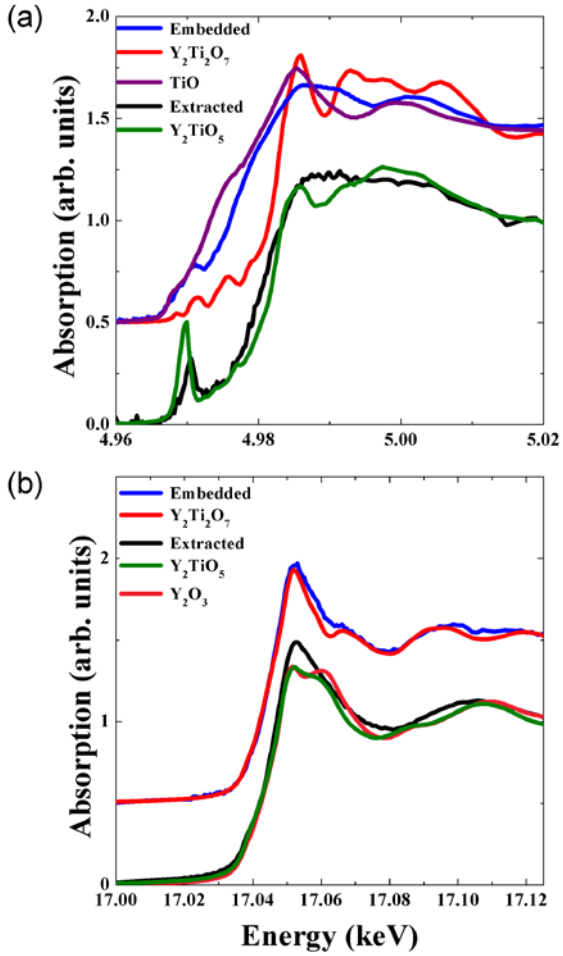

Figure 2. XANES spectra at the *K*-edge for (a) Ti and (b) Y for the embedded and extracted measurements. The TiO_2, Y_2O_3, Y_2TiO_5 and $Y_2Ti_2O_7$ bulk standards are shown for reference.

The magnitude of the Fourier Transformed EXAFS spectra, $|\chi(R)|$ ($Å^{-3}$), for the Ti and Y K-edges are shown in Figure 3a and Figure 3b, respectively. The groups of atoms that are the same radial distance from the absorbers (Ti or Y) are called a shell, and the number of atoms in the shell gives the coordination number. The Ti *K*-edge EXAFS data for the as-received MA957 (embedded) is complex, with multiple environments giving rise to the observed fine structure. For example, the first nearest neighbor at ~1.5 Å in the embedded spectra is attributed to Ti-O bonds (the large intensity is indicative of multiple environments); and the peak at ~2.5 Å is similar in position to the metallic Ti in solution. These features are consistent with previous studies where multiple environments were also observed [22]. The extracted EXAFS show significantly less structure at the Ti edge, with weak signal beyond ~2 Å. The Y *K*-edge EXAFS spectra (Figure 3b) show that atomic environments for the embedded NOs are complex with nearest neighbors shells at ~1.6, 2.4 and 3.4 Å, similar to a mixture of the $Y_2Ti_2O_7$, Y_2O_3 and Y_2TiO_5. The extracted NOs again have a different structure, more closely resembling that of the Y_2TiO_5 and Y_2O_3 phases. The heights of the nearest neighbor shells are, however, much lower in intensity compared to the standards potentially due to larger structural disorder and relatively small NO sizes.

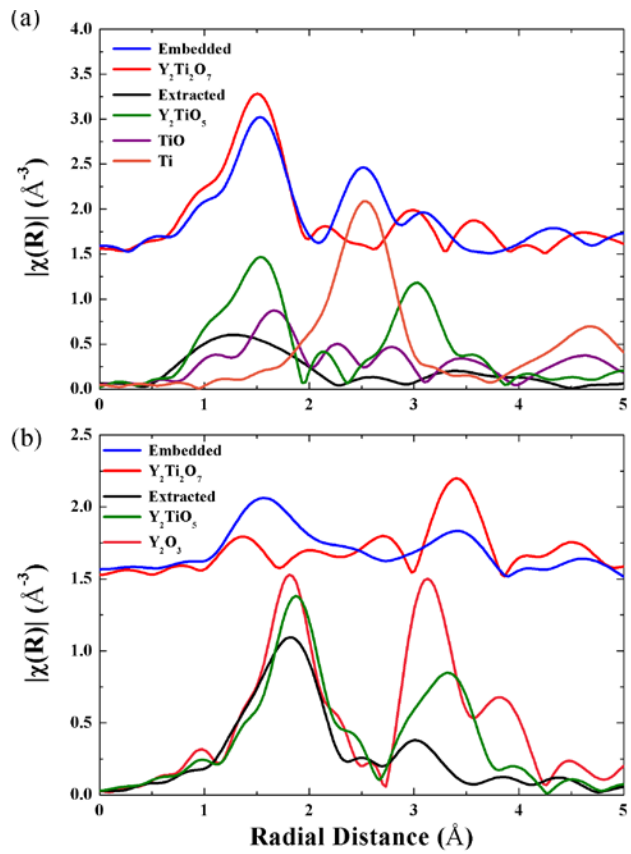

Figure 3. Fourier transform EXAFS for embedded, extracted and standards for (a) Ti *K*-edge and (b) Y *K*-edge.

The quantitative EXAFS fitting results in Table 1 show the coordination number (N), bond length (ΔBL), Debye – Waller factor ($\Delta\sigma^2$) and asymmetry parameter (ΔC_3) for the NOs as compared to standards. The relative changes in the structural parameters are also given for the different standards at both the Ti and Y *K*-edges. The Ti edge for the as-received (embedded) case has a large coordination number compared to the standards due to overlapping environments of the TiO and $Y_2Ti_2O_7$ phases. The changes in the Ti-O bond length were smaller for the $Y_2Ti_2O_7$ phase, consistent with the discussion above. The quantitative analysis at the Y edge indicates a mixture of the Y_2O_3 and $Y_2Ti_2O_7$ phases. However, the multiple overlapping environments in the embedded case (and large TiO and Y_2O_3 particles) hinder a full quantitative description of the structural parameters for both Ti and Y edges (note, this is not the ideal case for the model-independent method where an isolated first shell is needed).

The Ti *K*-edge quantitative results for the extracted NOs show a lower coordination number compared to the Y_2TiO_5 and TiO standards. An increase in the σ^2, slight bond length expansion and increase in asymmetry were also observed. The extracted NO structural parameters at the Y edge show similar trends, with a decrease in the coordination number, subtle changes in bond length and increase in σ^2. The results at both edges again indicate that the extracted NOs have a structure similar to Y_2TiO_5 phase (albeit with slightly different N, BL and σ^2). All the structural changes are consistent with the atomic environment commonly observed for NOs, where an increase in the surface-to-volume ratio results in an under-coordinated and reconstructed surface [27,28].

Table 1. Quantitative results from the EXAFS fitting indicating coordination number (N_{NO}/Ns), bond length (ΔBL), Debye – Waller factor ($\Delta\sigma^2$) and asymmetry parameter (ΔC_3). The subscripts NO and S are for Nano Oxide and Standard, respectively. *The embedded sample has multiple Ti and Y environments, and overlapping first nearest neighbor shells. The values for the embedded samples are an average of the multiple environments.

Nano Oxide	Edge	Standard	N_{NO}/N_S	$(BL_{NO} - BL_S)$ Å	$(\sigma^2_{NO} - \sigma^2_S)$ $x10^{-3}$ Å^2	$(C_{3NO} - C_{3S})$ $x10^{-4}$ Å^3
Embedded*	Ti	$Y_2Ti_2O_7$	0.96 (0.01)	0.0924 (0.001)	3.69 (0.13)	3.7 (0.3)
Embedded*	Ti	Y_2TiO_5	1.10 (0.05)	0.156 (0.001)	3.56 (0.13)	11.8 (0.2)
Embedded*	Y	Y_2TiO_5	0.64 (0.02)	0.058 (0.002)	4.74 (0.62)	34.8 (0.4)
Embedded*	Y	Y_2O_3	0.65 (0.03)	0.083 (0.001)	5.42 (0.7)	31.8 (0.3)
Extracted	Ti	Y_2TiO_5	0.55 (0.04)	0.039 (0.003)	2.93 (0.047)	15.4 (0.6)
Extracted	Ti	TiO	0.60 (0.03)	0.076 (0.002)	2.46 (0.037)	13.1 (0.4)
Extracted	Y	Y_2TiO_5	0.98 (0.07)	-0.005 (0.001)	4.82 (0.36)	2.7 (0.2)
Extracted	Y	Y_2O_3	0.87 (0.06)	0.037 (0.001)	8.05 (0.29)	2.9 (0.2)

The model-independent EXAFS analysis method is commonly used to extract atomic changes with temperature/pressure and has been used in both crystalline and amorphous materials [29]. The use of the method here, to quantify changes in nearest neighbor distances, is quite advantageous. The first atomic shell for the extracted NOs is well isolated (no multiple scattering paths overlap) and corresponds to common metal-oxygen bond. Thus, quantitative analysis yields information on the structural state of the NOs relative to the bulk standards. The combination of the qualitative XANES and quantitative EXAFS results clearly demonstrate that the extraction process is capable of isolating a minor component that is essentially overwhelmed by the large and complex environment observed when the NOs are embedded in a matrix.

The authors are aware that the extraction process may affect the character of the NOs. For example, possible segregation of Ti, O, and Cr to NO interfaces cannot be observed by XAS since the matrix is dissolved during extraction. Further, there may be some restructuring of the extracted NOs when they are released from the matrix. However, such extraction effects are not believed to be significant with respect to the core NOs, since they generally resemble those seen in TEM observations [6].

In conclusion, the chemistries and structures of NOs in NFA MA957 were characterized by XAS for both embedded and extracted precipitates. Measurements on embedded NOs in bulk MA957 are consistent with $Y_2Ti_2O_7$, while the slightly larger extracted oxides are primarily consistent with Y_2TiO_5. Analysis of the as-received MA957 was difficult due to the multiple Ti environments including $Y_2Ti_2O_7$, Y_2TiO_5, TiO, and dissolved metallic Ti. The bulk extraction and selective filtration technique successfully removed the matrix, trapped the larger Y_2TiO_5 particles, and yielded samples well suited for XAS measurements. The smaller $Y_2Ti_2O_7$ oxides passed through the filters but were the predominant embedded phase. This will be further confirmed in the future by XAS measurements on the residues in the filter effluent.

References

[1] G. R. Odette: *JOM*, 2014, vol. 66, p. 2427.
[2] G R Odette and D T Hoelzer: *JOM*, 2010, vol. 62, pp. 84–92.
[3] Steven J. Zinkle and Jeremy T. Busby: *Mater. Today*, 2009, vol. 12, pp. 12–19.
[4] N. Cunningham, Y. Wu, D. Klingensmith, et al.: *Mater. Sci. Eng. A*, 2014, vol. 613, pp. 296–305.
[5] Yuan Wu, Jim Ciston, Stephan Kräemer et al.: *Acta Mater.*, 2016, vol. 111, pp. 108–15.
[6] Y. Wu, E. M. Haney, N. J. Cunningham, et al.: *Acta Mater.*, 2012, vol. 60, pp. 3456–68.
[7] Joël Ribis, Eric Bordas, Patrick Trocellier, et al.: *J. Mater. Res.*, 2015, vol. 30, pp. 2210–21.
[8] S.Y. Zhong, J. Ribis, N. Lochet,et al.: *J. Nucl. Mater.*, 2014, vol. 455, pp. 618–23.

[9] J. Ribis and Y. De Carlan: *Acta Mater.*, 2012, vol. 60, pp. 238–52.
[10] V. Badjeck, M.G. Walls, L. Chaffron, et al.: *J. Nucl. Mater.*, 2015, vol. 456, pp. 292–301.
[11] Karl Dawson and Gordon J. Tatlock: *J. Nucl. Mater.*, 2014, vol. 444, pp. 252–60.
[12] N.J. Cunningham, Y. Wu, A. Etienne, et al.: *J. Nucl. Mater.*, 2014, vol. 444, pp. 35–38.
[13] Emmanuelle A. Marquis: *Appl. Phys. Lett.*, 2008, vol. 93, pp. 10–13.
[14] Ceri A. Williams, Paulina Unifantowicz, Nadine Baluc, et al.: *Acta Mater.*, 2013, vol. 61, pp. 2219–35.
[15] D. J. Larson, P. J. Maziasz, I-S Kim, et al.: *Scr. Mater.*, 2001, vol. 44, pp. 359–64.
[16] M.K. Miller, E.A. Kenik, K.F. Russell, et al.: *Mater. Sci. Eng. A*, 2003, vol. 353, pp. 140–45.
[17] M. Ohnuma, J. Suzuki, S. Ohtsuka, et al.: *Acta Mater.*, 2009, vol. 57, pp. 5571–81.
[18] Myriam Dumont, Lorelei Commin, Isabelle Morfin, et al.: *Mater. Charact.*, 2014, vol. 87, pp. 138–42.
[19] J.J. Fischer: Patent, Feb. 1978.
[20] N. J. Cunningham: *Thesis Univeristy Calif. St. Barbar.*, 2012.
[21] M.J. Alinger, G.R. Odette, and D.T. Hoelzer: *Acta Mater.*, 2009, vol. 57, pp. 392–406.
[22] S. Liu, G.R. Odette, and C.U. Segre: *J. Nucl. Mater.*, 2014, vol. 445, pp. 50–56.
[23] B Ravel and M Newville: *J. Synchrotron Radiat.*, 2005, vol. 12, pp. 537–41.
[24] Grant Bunker: *Nucl. Instruments Methods Phys. Res.*, 1983, vol. 207, pp. 437–44.
[25] L A Grunes: *Phys. Rev. B*, 1983, vol. 27, pp. 2111–31.
[26] Francois Farges, Gordon E Brown, and J J Rehr: *Phys. Rev. B*, 1997, vol. 56, pp. 1809–19.
[27] L L Araujo, R Giulian, D J Sprouster, et al.: *Phys. Rev. B*, 2008, vol. 78, p. 94112.
[28] Anatoly I. Frenkel, Charles W. Hills, and Ralph G. Nuzzo: *J. Phys. Chem. B*, 2001, vol. 105, pp. 12689–703.
[29] P Fornasini, S a Beccara, G Dalba, et al.: *Phys. Rev. B*, 2004, vol. 70, p. 174301.